Enhanced RBE of Particle Radiation Depends on Beam Size in the Micrometer Range

Authors: Ilicic, K., Dollinger, G., Dombrowsky, A., Greubel, C., Girst, S., et al.

Enhanced RBE of Particle Radiation Depends on Beam Size in the Micrometer Range

K. Ilicic,[a,b] G. Dollinger,[c] A. Dombrowsky,[a,b] C. Greubel,[c] S. Girst,[c] M. Sammer,[c] C. Siebenwirth,[b,c] E. Schmid,[d] T. Friedrich,[e] P. Kundrát,[e] W. Friedland,[a] M. Scholz,[e] S.E. Combs,[a,b] T.E. Schmid,[a,b] J. Reindl[c,1]

[a] Institute of Radiation Medicine (IRM), Helmholtz Zentrum München – German Research Center for Environmental Health, Neuherberg, Germany; [b] Department of Radiation Oncology, School of Medicine, Technische Universität München, Germany; [c] Institute for Applied Physics and Measurement Technology, Universität der Bundeswehr München, Neubiberg, Germany; [d] Department for Anatomy and Cell Biology, Ludwig-Maximilians Universität München, Germany; [e] GSI Helmholtz Center for Heavy Ion Research, Department of Biophysics, Darmstadt, Germany; [f] Department of Radiation Dosimetry, Nuclear Physics Institute of the Czech Academy of Sciences, Prague, Czech Republic

Ilicic K, Dollinger G, Dombrowsky A, Greubel C, Girst S, Sammer M, Siebenwirth C, Schmid E, Friedrich T, Kundrát P, Friedland W, Scholz M, Combs SE, Schmid TE, Reindl J. Enhanced RBE of Particle Radiation Depends on Beam Size in the Micrometer Range. Radiat Res. 201, 140–149 (2024).

High-linear energy transfer (LET) radiation, such as heavy ions is associated with a higher relative biological effectiveness (RBE) than low-LET radiation, such as photons. Irradiation with low- and high-LET particles differ in the interaction with the cellular matter and therefore in the spatial dose distribution. When a single high-LET particle interacts with matter, it results in doses of up to thousands of gray (Gy) locally concentrated around the ion trajectory, whereas the mean dose averaged over the target, such as a cell nucleus is only in the range of a Gy. DNA damage therefore accumulates in this small volume. In contrast, up to hundreds of low-LET particle hits are required to achieve the same mean dose, resulting in a quasi-homogeneous damage distribution throughout the cell nucleus. In this study, we investigated the dependence of RBE from different spatial dose depositions using different focused beam spot sizes of proton radiation with respect to the induction of chromosome aberrations and clonogenic cell survival. Human-hamster hybrid (A_L) as well as Chinese hamster ovary cells (CHO-K1) were irradiated with focused low LET protons of 20 MeV (LET = 2.6 keV/µm) beam energy with a mean dose of 1.7 Gy in a quadratic matrix pattern with point spacing of 5.4×5.4 µm² and 117 protons per matrix point at the ion microbeam SNAKE using different beam spot sizes between 0.8 µm and 2.8 µm (full width at half maximum). The dose-response curves of X-ray reference radiation were used to determine the RBE after a 1.7 Gy dose of radiation. The RBE for the induction of dicentric chromosomes and cell inactivation was increased after irradiation with the smallest beam spot diameter (0.8 µm for chromosome aberration experiments and 1.0 µm for cell survival experiments) compared to homogeneous proton radiation but was still below the RBE of a corresponding high LET single ion hit. By increasing the spot size to 1.6–1.8 µm, the RBE decreased but was still higher than for homogeneously distributed protons. By further increasing the spot size to 2.7–2.8 µm, the RBE was no longer different from the homogeneous radiation. Our experiments demonstrate that varying spot size of low-LET radiation gradually modifies the RBE. This underlines that a substantial fraction of enhanced RBE originates from inhomogeneous energy concentrations on the µm scale (mean intertrack distances of low-LET particles below 0.1 µm) and quantifies the link between such energy concentration and RBE. The missing fraction of RBE enhancement when comparing with high-LET ions is attributed to the high inner track energy deposition on the nanometer scale. The results are compared with model results of PARTRAC and LEM for chromosomal aberration and cell survival, respectively, which suggest mechanistic interpretations of the observed radiation effects. © 2024 by Radiation Research Society

INTRODUCTION

Effects of ionizing radiation generally depend on absorbed radiation dose, i.e., the deposited energy density on a macroscopic scale. However, the aspect of radiation quality, which is largely related to the concentration of energy deposited on a microscopic scale, is also of great importance for the biological effects. From this perspective, radiation quality includes the type of radiation, e.g., photons, ions or electrons, and their energy. In the case of ion radiation, the ion type and their kinetic energy are also associated with a linear energy transfer (LET) and a characteristic track structure, which specify the energy deposition on a microscopic scale. This microscopic dose distribution may strongly modulate the effect and is related to the relative biological effectiveness (RBE) for radiobiological endpoints (*1*) or particle therapy of cancer (*2, 3*), or used for designating radiation weighting factors by the ICRP for radiation protection purposes (*4*).

For clinical applications or in radiation protection, a relation between the RBE and the ion species, and LET is

140

required. Therefore, modeling of RBE as a function of the ion track structure received much attention. The radiation effect manifests itself as a result of a multiple process cascade ranging over various spatial scales, including physical, biochemical and biological aspects. It is therefore expected that various scales may play a role in modulating the effect. This has been quantitatively confirmed in our previous work (5) based on focused ion beams, where we pointed out that for carbon-ion beams, multiple scales must be considered simultaneously to understand the RBE. The coexistence of multiple processes on different spatial scales is therefore of paramount importance to consider in biological treatment planning for ion beam therapy. In turn, it is expected that model approaches considering only one spatial scale, e.g., either the μm or nm scale, will fail in describing the versatile dependence of RBE on the microscopic distribution of deposited energy. For a thorough RBE assessment, it is therefore desirable to understand the relevance of all contributing scales. In the present work, we specifically test the impact of energy deposition on the micrometer scale.

While in our previous work we have used a fixed focus width, in the present work we now investigate in more detail how the effect enhancement depends on the energy concentration on the μm scale by varying the focus width of the ion beam. A detailed knowledge of this would allow for interpretations about the interaction ranges of damage induction and repair processes. Ionizing radiation induces several types of DNA damage such as single-strand breaks, double-strand breaks (DSBs), base damage and DNA-protein cross links. These DNA damage types differ in their ability to be repaired and therefore affect the fate of the irradiated cell. Clustered DNA damage, which consists of two or more lesions on both DNA strands within a few base pairs of each other, is more difficult to repair (6). Thus they are more time-consuming for the cell to repair and lead to increased cell inactivation (7–10). In addition, DSBs on different chromosomes in close proximity increase the likelihood of misrejoining (11) and complex genetic damage, and this can impair cell survival (12). The clustered DNA damages (typically in nanometer dimensions) and enhanced numbers of damages on neighboring chromosomes in close proximity (with distances up to micrometers), are therefore considered as one reason for the increased biological effectiveness of high-LET radiation, as the highly localized dose deposition mainly causes these kinds of damage (13). That the damage clustering in the μm range has a major impact on enhancing RBE has also been demonstrated in our previous studies (5). Compared to the rather separated DSBs induced by low-LET radiation, the clustering results in a larger number of chromosome aberrations (CA) (14) and a reduction in the number of surviving cells (5).

Furthermore, in our recent work we have combined experimental studies with model calculations using PARTRAC and the local effect model (LEM) to investigate and interpret the

spatial extent of DNA lesion patterns that cause cell inactivation using focused beam spots of ionizing radiation (5, 14, 15). Our present experiments should help to clarify how the RBE is affected by the dose distribution on the micrometer scale, to obtain reliable knowledge about the RBE for any ion species as a function of its energy for both CA and cell survival. In contrast to former studies, where different ions were used to obtain varying dose distributions on the micrometer scale, a more direct approach is used in our study.

The aim of this study is to assess the influence of different beam spot sizes on the RBE with respect to clonogenic cell survival and CA. For this purpose, cells were irradiated with 1.7 Gy of low-LET 20 MeV protons using the ion microbeam SNAKE (Supraleitendes Nanoskop für angewandte kernphysikalische Experimente, or superconducting nanoprobe for applied nuclear physics experiments) at the Munich tandem accelerator (16, 17). The particles were either focused to a grid-like radiation pattern with 5.4 μm spot distance, where 117 protons were focused to different beam diameters ranging from 0.8 μm to 2.8 μm, or applied in a quasi-homogeneous field. Clonogenic cell survival and CA were determined after irradiation and the RBE was calculated for each irradiation geometry and end point by comparing data with data obtained using 70 kV X rays as the reference radiation. The results were then compared to Monte Carlo-based PARTRAC and LEM simulations, to aid in the interpretation of the data.

MATERIALS AND METHODS

Cell Culture for Chromosome Aberration Test

In the experiments, the A_L cell line was used, which has been established in our laboratory at the Technische Universität München (TUM) to investigate structural or functional CA after exposure to ionizing or non-ionizing radiation. This cell line was originally derived from the Chinese hamster ovary-K1 (CHO-K1) wild-type cell line, a subclone from an adult Chinese hamster (*Cricetulus griseus*). The A_L cells contain a standard set of CHO-K1 chromosomes plus a single human chromosome 11. Our previous chromosome analysis showed a modal number of 22 chromosomes (85% of analyzed cells); 15% of the analyzed cells had a loss or gain of chromosomes (18). The cells were grown as monolayer cultures in RPMI-1640 medium (Sigma Aldrich), supplemented with 16% fetal calf serum and antibiotics (100 units penicillin and 100 μg streptomycin per ml culture medium; Sigma Aldrich). The cell monolayers were maintained at 37°C in a humidified atmosphere of 5% CO_2 in air. Under these growth conditions, the A_L cells had a doubling time of 18 h. Special irradiation containers were used for all types of irradiations to fit the needs of the particle irradiation of cells at SNAKE. These cell containers were constructed in such a way that a Mylar foil (6 μm thick) was stretched and clamped between two steel plates. The design of the irradiation containers has been described previously (19). Approximately 24 h before exposure, cells were seeded on mylar foil pre-treated with Cell-TAK (Corning). Just before irradiation, the monolayer of cells was washed to remove any unattached cells.

Cell Culture for Clonogenic Cell Survival

The cell survival experiments were performed with the original CHO-K1 cell line, which is well established for colony forming assay (5). Cells were cultivated in RPMI-1640 medium (Sigma Aldrich) supplemented with 10% fetal calf serum (Sigma Aldrich), 100 units of Penicillin and 100 μg of Streptomycin per ml culture medium, 2 mM L-Glutamine and 1 mM Sodium pyruvate (Sigma Aldrich). The

cells were grown as a monolayer culture in an incubator at 37°C, 5% CO_2 and 95% humidity. Under these culture conditions the CHO-K1 cells had doubling time of ~12 h. Special irradiation containers were used for the particle irradiation of cells at SNAKE, as described above. For cell survival experiments, it is essential that all seeded cells are exposed, since unirradiated cells would alter the experimental outcome. For this purpose, the cell cultivation setup was modified and adapted for the application in microbeam irradiation experiments as described in detail by Greubel et al. (20).

Briefly, approximately 4 h before irradiation cells were seeded on mylar foil pre-coated with Cell-TAK (Corning) in an area at the center defined by an O-ring (4-mm diameter) (5). The total cell growth area was about 15 mm², which ensured a sufficient number of cells (~10⁴ cells) after irradiation and reseeding to analyze clonogenic cell survival. Directly before irradiation, the O-ring and its support were removed and cells were washed to get rid of all unattached cells.

Cell Irradiation with 20 MeV Protons

Ion irradiations were performed at the Scanning Ion Microprobe SNAKE installed at the Munich 14 MV tandem accelerator (21). Recent developments at SNAKE allowed focusing of particles to a minimum spot size of about 0.5×1.0 µm² with a particle rate of 200–500 kHz for protons (20). The protons were focused and transported in vacuum to the beam exit nozzle, which was covered with 7.5-µm thick Kapton foil. After passing the Kapton foil, the ions traversed a 6-µm thin Mylar foil before interacting with the cells. Behind the cell sample, a detector, as described by Hauptner et al. (16), was placed to count the ions. With this setup and an additional fast high-voltage beam switch, it is possible to irradiate with a known number of ions impinging a single spot. Using electrostatic beam scanning, single spots in a square field of 500×500 µm² were irradiated with a certain number of ions. The cell container was mounted on the XY stage of an inverted optical microscope (Zeiss Axiovert 200 M) (17) and by mechanically moving the cell sample, the square fields were stitched together to cover the entire area of cell growth. For a quasi-random proton irradiation, the microbeam was scanned over an area of 500×500 µm² with a scan rate much higher than the count rate, and protons were counted until the desired number of particles, and therefore the desired dose, was reached.

Before irradiation, about half of the culture medium was removed and the irradiation containers were tightly closed by clamping a second 6 µm Mylar foil. The exposure took place at room temperature (about 22°C). During irradiation, the container with the cell monolayer was positioned vertically in front of the beam exit nozzle with cells facing the microbeam. In this position, cells were not covered by culture medium, but the medium in the cell container prevented cells from drying out by ensuring a saturated atmosphere (16, 22).

Typically, the total time required for sample preparation and exposure was less than 25 min, including about 15 min in the upright position. Under these conditions, there were no differences in the number of observed chromosome aberrations in non-irradiated cells and cell samples remaining in the incubator (19). For cell survival, a sham-irradiated sample was used as control (where the sample was placed in the SNAKE setup for 15 min without switching on the beam) to exclude uncertainties in the data coming from the treatment in upright position.

Two independent experiments for chromosome aberrations (experiments I and II) and three for cell survival (experiments III, IV and V) were performed to demonstrate reproducibility as well as inter-test variability. Each irradiation was done using 20 MeV protons (LET = 2.6 keV/µm) not targeted to single cells but in a regular pattern of 5.4×5.4 µm spot distance for matrix irradiation using the same average dose of 1.7 Gy, which leads to 117 protons per point. Given the size of a CHO cell nucleus of 70 µm², the irradiation with a regular pattern of this size results in an average 2.4 ± 0.8 irradiated spots per nucleus (20). For the AL cells, a size of 117 µm² gives an average of 4.0 ± 0.2 hits per nucleus. A schematic image shows how the hits are distributed over the cells in Supplementary Fig. S1² (https://doi.org/10.1667/RADE-23-00217.1.S1). A histogram showing the fraction of cells with various doses are shown in

Supplementary Fig. S2 (https://doi.org/10.1667/RADE-23-00217.1.S2). Homogeneous dose was achieved by applying on average 4 ions per µm² in the quasi-homogeneous scan mode.

Spot irradiation was performed with three different spot sizes. The smallest beam spot was achieved by the best possible focusing, which varies for different beam times and also locally on the radiation field, due to external influences such as chromatic aberrations of the lens, beam position and electromagnetic interfering fields, to a full width at half maximum of 1.0×0.2 µm for colony forming and 0.78×0.01 µm for dicentric chromosomes, with the same dimensions in the x and y direction. The sample was placed in contact with the beam exit window to ensure irradiation with this small beam spot. The other two spot sizes were achieved by exploiting the scattering of the beam in the Kapton window. By moving the sample away from the beam exit at a certain distance, beam sizes of 1.80×0.15 µm and 2.80×0.18 µm for cell survival and 1.60×0.02 µm and 2.70×0.03 µm for CA were achieved. The difference in the spot sizes for cell survival and CA originate from the different minimal beam sizes, as the distance from the sample to the beam exit was kept the same. Beam spot size was measured as explained by Greubel et al. (20) using fluorescent nuclear track detectors (FNTDs). Briefly, 500×500 µm² fields with 5.4×5.4 µm spot distance were irradiated using the three different beam spot sizes inducing fluorescent color centers inside the FNTD crystals. After irradiation, the FNTDs were imaged using a Leica TCS SP8 3X confocal microscope with excitation at 635 nm and detection of fluorescent light between 645–740 nm and a pixel size of 50×50 nm² with a pixel dwell time of 24 µs and a resolution of approximately 200–250 nm. A Leica HCX PL APO100x/1.4 Oil objective with 100x magnification and numerical aperture of 1.4 was used. The spot size is determined by deconvolving the measured spots with the single ion response as described in detail by Greubel et al. (20). For size determination of the whole beam, nine regions from the field each containing 5×5 spots are analyzed, one from each corner, the center of the field and one in the middle of each side of the field. This is done to ensure coverage of all possible beam variations in x- and y-direction while keeping the effort practical. All 225 spots were then fitted using a two-dimensional Gaussian distribution with the full width at half-maxima representing the x- and y- beam spot size, where the y beam spot is ~25% larger than the x beam spot. From this data, the mean beam size in each direction is achieved from these two values, and the mean spot diameter is calculated. The provided error represents the standard deviation.

The reference X-ray irradiation was performed in the same cell dishes, with 200 kV X rays for cell survival (5) and 70 kV X rays for CA (14), as described before.

After Irradiation Culture and Chromosome Analysis

The cell culture conditions have been described in detail previously (12). The cells were trypsinized and reseeded in 4 ml RPMI-1640 medium supplemented with 20% fetal calf serum and antibiotics (penicillin/streptomycin) and incubated at 37°C in a humidified atmosphere of 5% CO_2 in air. Colcemid (Life Technologies Darmstadt, Germany) (0.1 µg/ml) was present in the cultures during the last 4 h of the total incubation time of 20 h. Chromosome preparation and Giemsa staining were carried out according to our standardized laboratory procedure originally described for human lymphocytes (23). All object slides were coded to ensure blinded evaluation. Only complete cells containing the modal number of 22 chromosomes were analyzed for dicentrics. Tricentric chromosomes were counted as two dicentrics, and similarly chromosomes with N > 3 centromeres, if present, were counted as N-1 dicentrics. Since the measured dicentric yields are generally used as the most characteristic and quantitatively reproducible biological endpoint of radiation-induced chromosome-type aberrations, only the data for

---

² Editor's note. The online version of this article (DOI: https://doi.org/10.1667/RADE-23-00217.1) contains supplementary information that is available to all authorized users.

dicentrics were used in the quantitative analysis, although the yields of centric rings and acentric fragments were also determined.

Survival Assay

Immediately after irradiation, the cells were disassociated from the mylar foil by trypsinization, and cell concentration from each sample was determined using the Fuchs-Rosenthal cell counting chamber (NanoEnTek). Cell counting was performed four times for each cell sample and the cell suspension was diluted in a dose-specific manner and reseeded into 12-well plates (Corning). In the case of the unirradiated (sham) samples, 100 cells were plated per well, while for the irradiated cell samples, 200 cells were reseeded per well. For each sample, cells were reseeded into wells of two to three 12-well plates, depending on the determined cell concentration. The plates were incubated under standard culture conditions until the cells had formed sufficiently large colonies, which consist of at least 50 cells (*24*). After five days, the medium was removed and cells were rinsed once with PBS. The colonies were fixed with methanol and stained with 0.1% crystal violet. The counting of stained colonies was performed by an automatic counting bioreader (BIO-SYS GmbH). In each experiment 5 replicates were used, and the focused data consist of 3 independent experiments, whereas for the homogeneous irradiation, five experiments were used.

Statistical Analysis of the Data

Dicentric Data Analysis. To test if the values for different spot sizes differ significantly, a statistical analysis is performed. A null hypothesis that the observations of the mean frequencies of dicentrics (±SE) determined in the independently performed experiments are not different was tested according to the z-test statistics. The intercellular distribution of dicentrics was tested for deviation from a Poisson distribution: A test quantity u has been used, which is related to the numbers of cells analyzed (N) and dicentrics scored (n) and the dispersion ratio (variance σ^2 over mean $y = n/N$) as described by Schmid et al. (*25*).

$$u = \left(\frac{\sigma^2}{y} - 1 \right) \sqrt{\frac{N-1}{2\left(1 - \frac{1}{n}\right)}} \qquad (1)$$

For a Poisson distribution, $\sigma^2 = y$ holds and hence $u = 0$. Values of u more than 1.96 indicate over-dispersion at the 5% level of significance.

Cell Survival Data Analysis. Cell survival data from multiple irradiated samples obtained from three beam times were available. The average effect, i.e., average of the negative logarithms of the survival, was determined from multiple irradiated samples within each

beam time. Uncertainties of the effects were calculated as the square root of the sum of effect variances for irradiated and control samples, the latter of which must be included as the control samples are used to calculate the plating efficiency. Thereby, retrieved effects from different beam times were pooled and average values for surviving fractions were calculated (see Table 1). Associated uncertfigainties for surviving fractions were determined by Gaussian error propagation as the square root of the uncertainty square sum. This pooling of data is justified as the spot sizes and all other conditions were comparable in the independent experiments carried out in the different beams. Hence. error bars and given uncertainty ranges in Table 1 are based on standard deviations and Gaussian error propagation, thus representing approximately 68% confidence intervals.

RBE Calculation. In the following calculations, the enhanced effect of the focused radiation is used. The RBE is calculated by identifying the dose of reference radiation necessary for achieving the same biological effect as the 1.7 Gy focused radiation. From this, the RBE is calculated as RBE = $D_{ref}/D_{focused}$, therefore the RBE for each focusing is determined for another level of biological effect.

To calculate the influence of the different spot size on the RBE for dicentrics, our previously established dose-response curve of dicentrics in A_L cells exposed to 70 kV X rays (*14*) was used. For this reference radiation quality, a weighted least-squares approximation was applied to fit the dicentric data with the linear-quadratic function. The resulting linear-quadratic coefficients (±SE) were $\alpha = (0.010 \pm 0.003)$ Gy^{-1} and $\beta = (0.0048 \pm 0.0012)$ Gy^{-2}. The dose-response curve of 200 kV X-ray irradiation of CHO-K1 cells established in a previous study (*5*) was used as a reference to determine the RBE for cell survival after random and focused proton irradiation. The linear quadratic coefficients $\alpha = (0.156 \pm 0.045)$ Gy^{-1} and $\beta = (0.0235 \pm 0.0055)$ Gy^{-2} and covariance Cov$(\alpha, \beta) = 0.00025$ Gy^{-3} were evaluated from the fit to the data points.

The reference radiation doses that caused effects equivalent to 1.7 Gy for random and focused proton irradiation of different beam spot sizes were determined by inverting the fitted dose-response curve with $-\ln(S)$, giving the effect for dicentrics induction or cell survival:

$$D(S) = \frac{-\alpha + \sqrt{\alpha^2 - 4\beta \ln S}}{2\beta} \qquad (2)$$

Associated uncertainties for the doses, ΔD were calculated according to Gaussian error propagation:

$$(\Delta D)^2 = \left(\frac{\partial D}{\partial \alpha} \Delta \alpha \right)^2 + \left(\frac{\partial D}{\partial \beta} \Delta \beta \right)^2 + \left(\frac{\partial D}{\partial S} \Delta S \right)^2 + 2 \frac{\partial D}{\partial \alpha} \frac{\partial D}{\partial \beta} Cov(\alpha, \beta) \qquad (3)$$

TABLE 1

Surviving Fractions (±SE) and RBE Values (±SE) for Cell Inactivation in CHO-K1 Cells after Exposure to 1.7 Gy of 20 MeV Protons either in Quasi Homogeneous Exposure Condition (P_{hom}) or in a Focused Mode Following a 5.4 × 5.4 µm² matrix (P_{foc}) at Different Beam Spot Sizes

Exposure to 20 MeV protons	Beam spot size (µm)	Mean cell survival fraction (±SE)	RBE (±SE)
Control	-	1.000 ± 0.06	-
P_{hom}	-	0.778 ± 0.046	0.788 ± 0.217
P_{foc}	0.85 ± 0.1	0.386 ± 0.056	2.27 ± 0.344
P_{foc}	1.0 ± 0.2	0.538 ± 0.057	1.646 ± 0.230
P_{foc}	1.8 ± 0.15	0.598 ± 0.066	1.422 ± 0.301
P_{foc}	2.8 ± 0.18	0.704 ± 0.059	1.046 ± 0.311

Notes. The mean value of homogeneous proton radiation was obtained from five independent experiments, whereas the mean values of focused proton irradiations were obtained from three independent experiments. In each experiment, each spot size contained five replicates. For the calculation of mean values of homogeneous irradiation, the data from three independently performed experiments were pooled together with data from homogeneous proton irradiation (*5*). The mean values of the 0.85 µm beam spot size were adopted (*5*) as well. For RBE calculation 200 kVp X rays were used. The RBE values presented are calculated for different biological effects as described in the text.

TABLE 2
Frequency (±SE) of Chromosome Aberrations and the Intercellular Distribution of Dicentrics in A_L Cells after Exposure to 1.7 Gy of 20 MeV Protons either in Quasi-Homogeneous Exposure Condition (P_{hom}) or in a Focused Mode Following a 5.4 × 5.4 μm² Matrix (P_{foc}) At Different Step Numbers

Exposure to 20 MeV protons		Cells scored	Dicentrics per cell (±SE)	Intercellular distribution of dicentrics					Centric rings per cell	Acentrics per cell
Matrix	Beam spot size [μm]			0	1	2	σ^2/y	u-value		
Mean values of experiment I										
P_{hom}		374	0.043 ± 0.011	359	14	1	1.09	1.27	0.027	0.091
P_{foc}	0.83 ± 0.02	876	0.086 ± 0.010	803	71	2	0.97	-0.65	0.047	0.145
P_{foc}	1.56 ± 0.03	657	0.078 ± 0.011	610	43	4	1.08	1.46	0.049	0.152
P_{foc}	2.73 ± 0.04	625	0.051 ± 0.009	593	32	0	0.95	-0.88	0.032	0.102
Mean values of experiment II										
P_{hom}		565	0.046 ± 0.010	541	22	2	1.11	1.88	0.011	0.085
P_{foc}	0.73 ± 0.02	689	0.083 ± 0.012	637	47	5	1.10	1.78	0.036	0.153
P_{foc}	1.64 ± 0.02	521	0.059 ± 0.017	490	30	1	1.00	0.05	0.031	0.127
P_{foc}	2.67 ± 0.03	644	0.047 ± 0.009	616	26	2	1.09	1.64	0.028	0.115
Mean values of the results obtained in experiment I and II										
P_{hom}		939	0.045 ± 0.007	900	36	3	1.10	2.18	0.017	0.087
P_{foc}	0.78 ± 0.01	1,565	0.085 ± 0.007	1,440	118	7	1.02	0.62	0.042	0.148
P_{foc}	1.60 ± 0.02	1,178	0.072 ± 0.01	1,100	73	5	1.05	1.23	0.041	0.141
P_{foc}	2.70 ± 0.03	1,269	0.049 ± 0.006	1,209	58	2	1.02	0.42	0.030	0.109

Note. The beam size is also given with ± SE.

Biophysical Effect Modeling

PARTRAC Simulation. PARTRAC (*26–30*) is a suite of Monte Carlo codes for biophysical modeling of radiation effects at subcellular and cellular levels. Radiation track structures, i.e., energy deposition patterns with single-event resolution, are generated by simulating individual interactions of photons, electrons, protons or ions with the traversed medium, using cross section data based on the work from Dingfelder et al. (*31*). Production of reactive species, their diffusion and mutual reactions are followed. Initial radiation-induced damage to DNA is scored, considering both direct energy depositions and indirect effects via attacks of reactive species. Multi-scale chromatin models are implemented that range from DNA in atomic resolution over its binding to nucleosomes, formation of chromatin fibers and loops, to chromatin domains and chromosome territories within human cell nuclei. The repair of DNA DSB via the non-homologous end-joining pathway (NHEJ) is modeled, explicitly accounting for both the kinetics of enzymatic processes and the mobility of individual broken ends. Chromosome aberrations and in particular dicentrics that result from misrejoining events are scored.

In this work, irradiation of A_L cells with 20 MeV protons was simulated with PARTRAC under diverse focusing modes as used in the experiments. In quasi-homogeneous irradiation, single protons per point were started in a matrix mode with a small grid size of 0.5 μm; the actual tracks were allowed to deviate from the grid points according to a Gaussian distribution with a comparably large spot size (full width at half-maximum) of 1.41 μm. For the three degrees of focusing, the spot size amounted to 2.70, 1.60 or 0.78 μm, respectively, always with 117 protons per spot and a grid size of 5.4 μm. The chromatin structure of A_L cells was approximated using two copies of chromosomes 1–11 from human lymphocytes (*15*). Standard PARTRAC modules and parameters were used to simulate particle tracks, reactive species, and induction of initial DNA damage as described previously (*27*). The model parameters were first optimized for this project as previously published (*28*). From there, further optimizations were performed (*15*), which were then used to predict the outcome in this study. Here, we used the NHEJ model (without hypothetical repair centers) to simulate the DNA repair. For each irradiation scenario, 500 runs were simulated, each

corresponding to matrix irradiation of a single cell. The induction of dicentrics within 24 h postirradiation was analyzed.

LEM Simulation. The LEM is a simulation tool, which predicts the effect of ionizing radiation based on two properties: the amorphous track structure and the photon dose response curve for the experimental endpoint. The amorphous track structure is the local dose deposited by an ion as a continuous function. reflecting the expected local energy concentration of a large ensemble of particle tracks. The photon dose response is characterized by the α and β values coming from linear-quadratic fitting and a threshold dose, which marks the transition to a linear regime and is set to $D_t = 4$ Gy + 1.1 α/β. A detailed description of the model approach can be found in the published literature (*5, 32*). The model was adapted to be able to predict the effect of single Gaussian shaped beam spots in cell nuclei (*5*) by considering the geometrical properties of the beam and the cell nuclei. The LEM simulations were performed separately for 33 beam sizes from 0.12 μm to 3.96 μm in 0.12 μm steps, assuming a round beam shape.

RESULTS

Dicentric Data

The detailed experimental results for dicentrics and their intercellular distribution in A_L cells are presented in Tables 1 and 2 together with the corresponding background frequencies. The spontaneous frequency in unirradiated cells of 0.0007 ± 0.0003 per cell determined in 4,500 cells (Table 2) is not statistically different from the value of 0.0006 ± 0.0003 dicentrics per cell obtained in 5,312 cells reported earlier (*19*). No significant differences have been determined between the yields of dicentrics, which were observed in any exposure mode between experiments I and II [P values (one-sided T-test) from 0.30 to 0.90] listed in Table 2. Therefore, the yields of dicentrics from the replicates within the different experiments were pooled. The
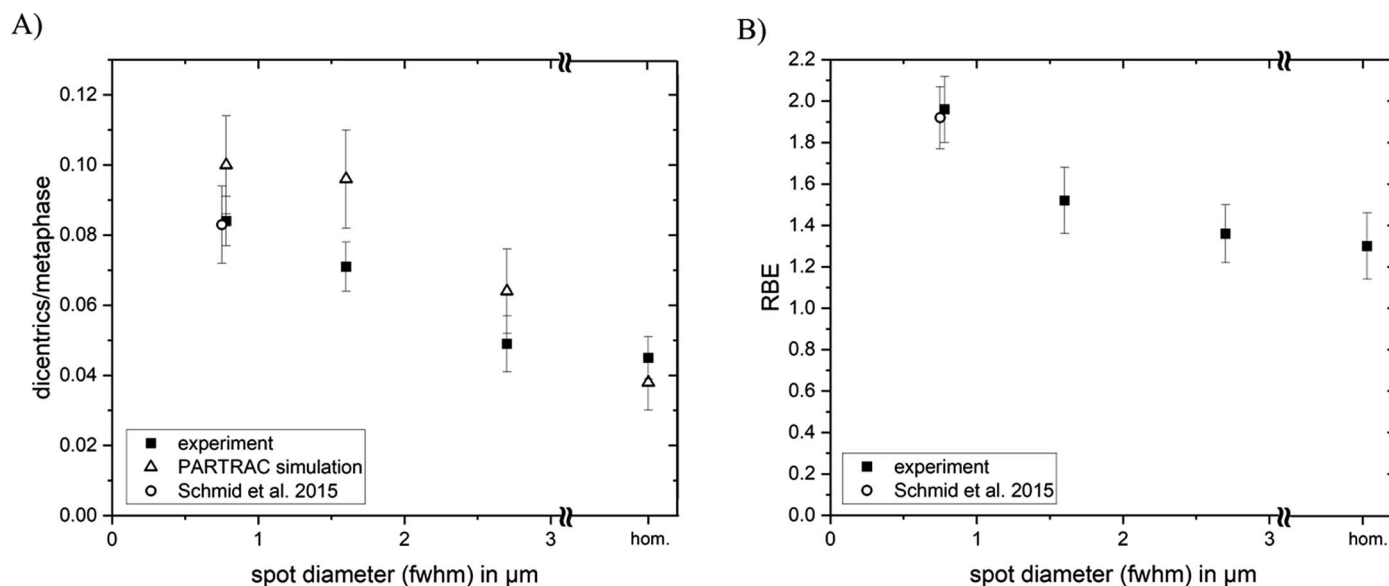
FIG. 1. Panel A: Comparison of PARTRAC simulation (triangles) and experiment (squares) for dicentrics induction at different spot sizes. Mean values representing measuring data from two proton beam times with three replicates per spot size and beam time are shown. For further comparison, data from Schmid et al. (*14*) are added, which nicely fit the actual experiment. One has to note that in this case an elliptical beam was used, and the spot diameter was calculated as the mean of the x (0.5 μm) and y width (1.0 μm). Error bars for the data points represent the standard errors (SE); Panel B: Relationship between RBE for the induction of dicentric chromosomes and spot size.

resulting mean values of dicentrics are plotted in Fig. 1A. The highest degree of focusing to a 0.78 μm beam spot increases the induction of dicentrics almost twofold compared to the quasi-homogeneous case. These enhancement factors decrease with decreasing degree of focusing. The data can also be compared with the data collected in a previous study (*14*). There, an elliptical spot of a size of 0.5 μm × 1.0 μm was applied, and a dicentrics induction of 0.083 ± 0.008 dicentrics/metaphase was observed. These data are well corresponding with the measurements performed in this study.

The RBE values were calculated using the X-ray doses that produced the same response as 1.7 Gy of the presently applied radiation qualities as explained in the Materials and Methods section. The resulting mean RBE values of dicentrics in experiments I and II are plotted in Fig. 1B. The RBE values are significantly higher when 117 protons were focused to a 0.78 μm spot within a 5.4×5.4 μm² matrix compared to homogeneously applied protons ($RBE_{0.78} = 1.96 \pm 0.16$ vs. $RBE_{hom} = 1.30 \pm 0.16$). By doubling the spot size to 1.6 μm, the RBE decreased to $RBE_{1.6} = 1.52 \pm 0.16$. By further increasing the spot size to 2.7 μm, the RBE was no longer different ($RBE_{2.7} = 1.36 \pm 0.14$) from the homogeneous radiation, yet above unity.

The measured data of dicentric induction were compared to the dicentric yields predicted by PARTRAC simulation (Fig. 1A). The simulation was performed based on the parameter values detailed in a previous study (*15*) and without further optimization and without knowledge of the present biological results, i.e., only-spot diameters as measured in the experiments and number of particles per spot were known. For homogeneous irradiation, PARTRAC

predicts a slightly lower number of dicentrics per metaphase than measured. For the focused geometry, PARTRAC is able to predict the trend that dicentric induction is increasing with increasing degree of focusing, i.e., with decreasing spot size. Between the smallest spot (0.78 μm) and the largest spot (2.7 μm), a reduction in the predicted frequency of dicentrics induction from 0.10 to 0.064 corresponds to a 1.6-fold decrease. Compared to homogeneous proton distribution, this corresponds to a 2.6-fold increase for the smallest spot size. In total, the dicentrics induction for the focused irradiation geometry is systematically overestimated between 20% and 30% by simulation compared to measurement, and slightly underestimated for homogeneous irradiation, while individual data points coincide within the uncertainties except for one.

Cell Survival Data

To calculate the influence of the different spot sizes on the RBE for cell survival, our previously established dose-response curve of cell survival in CHO-K1 cells exposed to 200 kV X rays was used, and the corresponding survival data of two independent experiments are shown elsewhere (*5*). The cell survival rates after microbeam exposure from three different beam times were pooled and average values for surviving fractions were calculated (Table 1) and plotted in Fig. 2A. The value from exposure of cells to a mean dose of 1.7 Gy of homogeneously applied protons resulted in 78% ± 5% cell survival. The highest degree of proton focusing to a 1.0-μm beam spot reduces the surviving fraction to 54% ± 6%. By increasing the beam spot size to 1.8 μm and 2.8 μm, the surviving fraction was increased to 60% ± 7% and 70% ± 6%, respectively. The data can be compared to data from a previous study (*5*) with the same
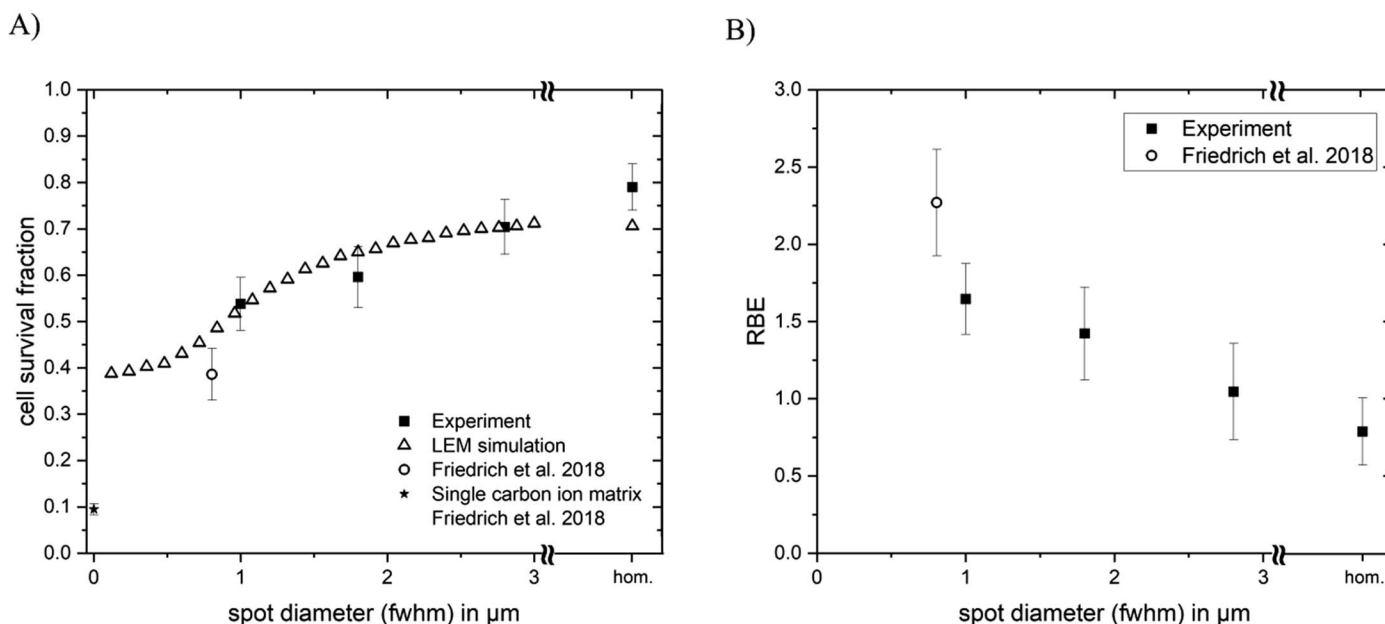
A)

B)

FIG. 2. Panel A: Comparison of LEM simulation (triangles) and experiment (squares) for cell survival at different spot sizes. The mean value of homogeneous proton irradiation was obtained from five independent experiments, whereas the mean values of focused proton irradiations were obtained from three independent experiments. In each experiment each spot size contained five replicates. For comparison, the data point of Friedrich et al. (5) for protons and single carbon ions (55 MeV, LET = 338 keV/μm) was added. Error bars for the data points represent the standard errors (SE); Panel B: Relationship between RBE for cell inactivation and spot size.

setup, where an elliptical beam was used, with width in x-direction of 0.56 ± 0.05 μm and y-direction of 1.1 ± 0.06 μm. For comparison the beam size of 0.81 ± 0.1 μm, was calculated as the mean of the width in x and y direction. Here a surviving fraction of 39% ± 6%, was measured, which shows that for even smaller focusing, cell killing is further enhanced.

The RBE values for cell inactivation were calculated using the X-ray doses that produced the same response as 1.7 Gy of the presently applied radiation qualities and the necessary X-ray doses have been determined by inverting the fitted dose-response curve. The resulting mean RBE values for cell survival are plotted in Fig. 2B.

The RBE for homogeneous proton radiation was 0.79 ± 0.2, which was not expected due to the common paradigm of an RBE of close to 1 for proton radiation, but is in agreement with previous results (5). The RBE was enhanced to 1.65 ± 0.25 after focusing protons to the smallest beam spot of 1-μm diameter. The RBE for cell inactivation using wider beam spots of 1.8 μm and 2.8 μm decreased to 1.42 ± 0.30 and 1.05 ± 0.31, respectively. The increased RBE can now be compared to the RBE of single carbon ion hits (RBE = 8.31 ± 0.21). It is notable that the increase of RBE by focusing to 1μm diameter covers approximately 20% of the increased RBE covered by the single ion hits with the same LET.

The measured cell survival data were compared to simulation using the LEM model (Fig. 2A). Notably, the simulation was performed without any specific parameter optimization and without prior knowledge of the biological data, using only the specific information that the spot should be considered round and 117 protons per spot are used. Therefore a

true prediction of the results was performed using the model as it was optimized based on the data from Friedrich et al. (5). The spot size was varied between 0.12 μm and 3.96 μm in 0.12 μm steps. For spot sizes below 0.5 μm, the predicted surviving fraction was almost constant at ~40%. After that, there was a steep increase with increasing spot size up to a 1 μm spot size, and the curve flattened towards even larger spot diameters. At 2-μm spot size, a slight increase of survival fraction was still visible but surviving fractions were already comparable to the results for the simulation of homogeneous irradiation. The simulation data agreed reasonably with the measured surviving fractions and the general trend of the shape and magnitude of the increase. However, for homogeneous irradiation, the LEM simulation tends to underestimate cell survival and for the smallest beam spot size the LEM overestimates the survival fraction compared to the experiments. One has to note, however, that this latter data point originates from a previous study, in which irradiation was performed with an elliptical spot (axes of 0.56 μm and 1.05 μm) rather than a round spot (5).

DISCUSSION

The aim of our study was to investigate the effect of different beam spot sizes on the RBE in terms of surviving fraction and CA. The RBE is an important parameter to be considered in radiotherapy of patients treated with ion beams (33). Radiotherapy using ion beams (currently mostly protons and carbon ions are used clinically), is advantageous for the treatment of some radioresistant tumors, and the number of particle treatment facilities is

increasing worldwide (*34*). The main physical difference between conventional low-LET-photon radiation and high-LET-ion beam radiation is the macroscopic and microscopic spatial dose deposition pattern. It is commonly assumed that low-LET radiation has an RBE ∼1. While isolated DNA damage as primarily induced by low-LET radiation can be efficiently repaired, clustered or complex lesions, as mainly induced by high-LET radiation, may be much more difficult and more time-consuming to repair.

Our experiments show that the increased RBE of heavier ions such as carbon ions for the induction of dicentrics and clonogenic cell survival can be mimicked partially by focused low-LET radiation, and that the increase in RBE is dependent on the focus size. The dose distribution of the focused protons differed significantly from that of quasi-homogeneous proton irradiation as shown previously (*5*). In our new study, the relationship between the RBE and the local dose distribution on the micrometer scale was studied in detail. By gradually focusing the protons, the local dose distribution could be modulated in a defined and quantitative way. Single proton tracks cluster in space and lead to enhanced yields of dicentric chromosomes by inter-track interaction in a similar way as by intra-track effects of high-LET radiation. The same process also leads to a reduction of clonogenic cell survival. The smaller the focusing, the more damage clustering is achieved. Notably, although the focusing to a submicrometer beam spot lead to an enhanced RBE, 80% of the enhancement of single hits from ions with the same LET as the focused spots came from the nanometer scale.

In that respect our experiments complement earlier experiments that also aimed to analyze the impact of inter-track interaction on the effectiveness of ion beam radiation. In these experiments, molecular beams of diatomic deuterium were used, and spatially correlated deuterium ions were produced by break-up of the molecules within thin target foils (*35, 36*). The distance between the individual, correlated atoms could then be controlled within certain limits by varying the thickness of the target foil and the corresponding variation in scattering, leading to an increased separation with increasing target foil thickness. Further experiments were performed be Geard et al. (*37*), where three protons with an average distance of 0.2 µm were applied to ovarian hamster V79 cells. The effect of inducing chromosomal aberrations was scored and showed a 52% enhanced effect of the triads of particles. Despite the technical limitations of these early experiments, they also showed a slight trend toward increased effectiveness with decreasing separation between the correlated atoms (*37, 38*).

Conventional experiments on radiobiological effects of radiation types differing in their LET cannot separate the relative importance of the micrometer scale DSB clustering from the inherently interlinked clustering on the nanometer scale relevant for DSB induction. However, sub-micrometer focusing of protons enables separating these scales by comparing

with heavier ions at the same total energy deposition and correspondingly lower number of ions per spot, as demonstrated in Friedrich et al. (*5*). For comparison, the data for carbon-radiation exposure were also included in Fig. 2; focusing modified the spatial distribution of DSB on the micrometer scale, while the high energy concentration on the nanometer scale within carbon ion tracks also caused an elevated DSB yield. We showed that the micrometer scale contributes to the enhanced effectiveness of heavy ions, in this case by 20%. Our data, together with the data from Friedrich et al. (*5*) provide direct experimental evidence that both scales are relevant for the induction of dicentrics and cell killing.

Due to the strong dependence of RBE on the ion species and energy as well as tissue type, different models have been developed to account for the complex dependencies of RBE on many factors. The local effect model (LEM) is in its original version in clinical use for RBE predictions at European carbon ion centers, and the current version LEM IV (*39*) used here allows an interpretation of the relevant scales based on explicit DSB simulations. Our results support the assumption of the LEM that the microscopic spatial dose distribution on the micrometer and nanometer scale is the main source of relative biological effectiveness (*5*). In addition, track structure-based simulations of DSB induction and chromosome aberration formation are also performed using PARTRAC, a stochastic Monte Carlo-based modeling tool for simulating biological effects of ionizing radiation (*26*). PARTRAC calculations start with simulating the track structure of the radiation considered (photons, electrons, ions) by following step-by-step the interactions of the primary particle and all secondary particles within a region of interest. This study shows direct experimental evidence that clustering of DSB in the micrometer scale plays a critical role in the induction of dicentrics, which was also reproduced by PARTRAC calculations.

In conclusion, in our experiments, we gradually varied the spot size of low-LET protons at ∼1 µm, which allowed us to scan one of the important scales for enhanced RBE regarding cell killing and dicentrics induction. We showed that focusing of beams to ∼1 µm has a major impact on cell survival, as gradually focusing a beam from homogeneous irradiation to 0.85 µm spot size results in a ∼3-fold increase in RBE. LEM simulations predict a plateau for smaller spot sizes, which may indicate the difference of a µm-focused beam and a single high-LET particle depositing the same energy. As known from the general limitations of microdosimetry (*40*), the energy deposition of a single high LET particle is relevant also in even smaller volumes, which adds the nanometer scale to the dose response. This has been investigated and verified in our previous study, where the difference in effect between strongly-focused proton spots and carbon ions was traced back to lesion formation on the nm scale (*5*).

To further study the RBE enhancement mechanisms on different scales in experiments, it would also be necessary

to temporally focus the beam. This has not been pursued to date and would require, in addition to focusing capabilities, a methodology to precisely shape the temporal radiation delivery. In the present work, we considered the impact of spatial radiation patterns, particularly on the micrometer scale, and found a clear dependence of the RBE on the degree of focusing. This directly supports the idea of stronger lesion formation fostered by large local (i.e. spread on the micrometer scale) ionization densities.

SUPPLEMENTARY INFORMATION

Fig. S1. Overlay between a theoretical irradiation pattern with spot distances of 5.4 μm in x and y direction with a microscopic image of CHO cell nuclei stained with DAPI.

Fig. S2. Fraction of cells irradiated with various doses (CHO cells = black; A_L cells = orange). The distribution comes from the size and spatial distribution of the cell nuclei and the beam.

ACKNOWLEDGMENT

REFERENCES

1. Franken NAP, ten Cate R, Krawczyk PM, Stap J, Haveman J, Aten J, et al. Comparison of RBE values of high-LET α-particles for the induction of DNA-DSBs, chromosome aberrations and cell reproductive death. Radiat Oncol 2011; 6:64.

2. Kraft G. RBE and its interpretation. Strahlenther Onkol 1999; 175 Suppl 2:44–47.

3. Gerweck LE, Kozin SV. Relative biological effectiveness of proton beams in clinical therapy. Radiother Oncol 1999; 50:135–42.

4. Charles MW. ICRP Publication 103: Recommendations of the ICRP. Radiat Prot Dosimetry 2007; 129:500–07.

5. Friedrich T, Ilicic K, Greubel C, Girst S, Reindl J, Sammer M, et al. DNA damage interactions on both nanometer and micrometer scale determine overall cellular damage. Sci Rep 2018; 8: 16063.

6. Mladenov E, Iliakis G. Induction and repair of DNA double strand breaks: the increasing spectrum of non-homologous end joining pathways. Mutat Res 2011; 711:61–72.

7. Goodhead DT. Mechanisms for the biological effectiveness of high-LET radiations. J Radiat Res 1999; 40 Suppl:1–13.

8. Goodhead DT, Thacker J, Cox R. Weiss Lecture. Effects of radiations of different qualities on cells: molecular mechanisms of damage and repair. Int J Radiat Biol 1993; 63:543–56.

9. Schmid TE, Dollinger G, Beisker W, Hable V, Greubel C, Auer S, et al. Differences in the kinetics of gamma-H2AX fluorescence decay after exposure to low and high LET radiation. Int J Radiat Biol 2010; 86:682–91.

10. Zlobinskaya O, Dollinger G, Michalski D, Hable V, Greubel C, Du G, et al. Induction and repair of DNA double-strand breaks assessed by gamma-H2AX foci after irradiation with pulsed or continuous proton beams. Radiat Envir Biophys 2012; 51:23–32.

11. Hagiwara Y, Oike T, Niimi A, Yamauchi M, Sato H, Limsirichaikul S, et al. Clustered DNA double-strand break formation and the repair pathway following heavy-ion irradiation. J Radiat Res 2019; 60:69–79.

12. Mavragani IV, Nikitaki Z, Kalospyros SA, Georgakilas AG. Ionizing Radiation and Complex DNA Damage: From Prediction to Detection Challenges and Biological Significance. Cancers 2019; 11.

13. Nickoloff JA, Sharma N, Taylor L. Clustered DNA Double-Strand Breaks: Biological Effects and Relevance to Cancer Radiotherapy. Genes 2020; 11.

14. Schmid TE, Friedland W, Greubel C, Girst S, Reindl J, Siebenwirth C, et al. Sub-micrometer 20MeV protons or 45MeV lithium spot irradiation enhances yields of dicentric chromosomes due to clustering of DNA double-strand breaks. Mutat Res 2015; 793:30–40.

15. Friedland W, Kundrát P, Schmitt E, Becker J, Ilicic K, Greubel C, et al. Modeling studies on dicentrics induction after sub-micrometer focused ion beam grid irradiation. Radiat Prot Dosimetry 2019; 183: 40–44.

16. Hauptner A, Dietzel S, Drexler GA, Reichart P, Krücken R, Cremer T, et al. Microirradiation of cells with energetic heavy ions. Radiat Environ Biophys 2004; 42:237–45.

17. Hable V, Greubel C, Bergmaier A, Reichart P, Hauptner A, Krücken R, et al. The live cell irradiation and observation setup at SNAKE. Nuclear Instruments and Methods in Physics Research Section B: Beam Interactions with Materials and Atoms 2009; 267:2090–97.

18. Schmid TE, Dollinger G, Hable V, Greubel C, Zlobinskaya O, Michalski D, et al. The effectiveness of 20 mev protons at nanosecond pulse lengths in producing chromosome aberrations in human-hamster hybrid cells. Radiat Res 2011; 175:719–27.

19. Schmid TE, Greubel C, Hable V, Zlobinskaya O, Michalski D, Girst S, et al. Low LET protons focused to submicrometer shows enhanced radiobiological effectiveness. Phys Medi Biol 2012; 57: 5889–907.

20. Greubel C, Ilicic K, Rösch T, Reindl J, Siebenwirth C, Moser M, et al. Low LET proton microbeam to understand high-LET RBE by shaping spatial dose distribution. Nuclear Instruments and Methods in Physics Research Section B: Beam Interactions with Materials and Atoms 2017; 404:155–61.

21. Datzmann G, Dollinger G, Goeden C, Hauptner A, Körner H-J, Reichart P, et al. The Munich microprobe SNAKE: First results using 20 MeV protons and 90 MeV sulfur ions. Nuclear Instruments and Methods in Physics Research Section B: Beam Interactions with Materials and Atoms 2001; 181:20–26.

22. Greubel C, Hable V, Drexler GA, Hauptner A, Dietzel S, Strickfaden H, et al. Quantitative analysis of DNA-damage response factors after sequential ion microirradiation. Radiat Environ Biophys 2008; 47:415–22.

23. Agrawala PK, Adhikari JS, Chaudhury NK. Lymphocyte chromosomal aberration assay in radiation biodosimetry. J Pharmacy Bioallied Sci 2010; 2:197–201.

24. Franken NAP, Rodermond HM, Stap J, Haveman J, van Bree C. Clonogenic assay of cells in vitro. Nature Protocols 2006; 1: 2315–19.

25. Schmid E, Braselmann H, Nahrstedt U. Comparison of γ-ray induced dicentric yields in human lymphocytes measured by conventional analysis and FISH. Mutat Res 1995; 348:125–30.

26. Friedland W, Kundrát P, Jacob P. Stochastic modelling of DSB repair after photon and ion irradiation. Int J Radiat Biol 2012; 88: 129–36.

27. Friedland W, Dingfelder M, Kundrát P, Jacob P. Track structures, DNA targets and radiation effects in the biophysical Monte Carlo simulation code PARTRAC. Mutat Res 2011; 711:28–40.

28. Friedland W, Kundrát P. Track structure based modelling of chromosome aberrations after photon and alpha-particle irradiation. Mutat Res 2013; 756:213–23.

29. Kundrát P, Friedland W, Becker J, Eidemüller M, Ottolenghi A, Baiocco G. Analytical formulas representing track-structure simulations on DNA damage induced by protons and light ions at radiotherapy-relevant energies. Sci Rep 2020; 10:15775.

30. Friedland W, Kundrát P. Chromosome aberration model combining radiation tracks, chromatin structure, DSB repair and chromatin mobility. Radiat Prot Dosimetry 2015; 166:71–74.

31. Dingfelder M, Ritchie RH, Turner JE, Friedland W, Paretzke HG, Hamm RN. Comparisons of calculations with PARTRAC and NOREC: transport of electrons in liquid water. Radiat Res 2008; 169:584–94.

32. Friedrich T, Scholz U, Elsässer T, Durante M, Scholz M. Calculation of the biological effects of ion beams based on the microscopic spatial damage distribution pattern. International journal of radiation biology 2012; 88:103–07.

33. Howard M, Beltran C, Sarkaria J, Herman MG. Characterization of relative biological effectiveness for conventional radiation therapy: a comparison of clinical 6 MV X-rays and 137Cs. J Radiat Res. 2017; 58:608–13.

34. Stewart RD, Carlson DJ, Butkus MP, Hawkins R, Friedrich T, Scholz M. A comparison of mechanism-inspired models for particle relative biological effectiveness (RBE). Med Phys 2018; 45:e925-e952.

35. Kellerer AM, Lam Y-MP, Rossi HH. Biophysical Studies with Spatially Correlated Ions: 4. Analysis of Cell Survival Data for Diatomic Deuterium. Radiat Res 1980; 83:511.

36. Colvett RD, Rohrig N. Biophysical Studies with Spatially Correlated Ions: 2. Multiple Scattering, Experimental Facility, and Dosimetry. Radiat Res 1979; 78:192.

37. Geard CR, Colvett RD, Rohrig N. On the mechanics of chromosomal aberrations: a study with single and multiple spatially-associated protons. Mutat Res 1980; 69:81–99.

38. Bird RP. Biophysical Studies with Spatially Correlated Ions 3. Cell Survival Studies Using Diatomic Deuterium. Radiat Res 1979; 78:210.

39. Elsässer T, Weyrather WK, Friedrich T, Durante M, Iancu G, Krämer M, et al. Quantification of the relative biological effectiveness for ion beam radiotherapy: direct experimental comparison of proton and carbon ion beams and a novel approach for treatment planning. Int J Radiat Oncol Biol Phys 2010; 78: 1177–83.

40. Lindborg L, Waker A. Microdosimetry: Experimental methods and applications. Boca Raton, FL: CRC Press Taylor & Francis Group; 2017.